# Effect of Sb and Na incorporation in $Cu_2ZnSnS_4$ solar cells

Md Abdul Aziz Suzon[a,b], Louis Grenet[a,b,*], Fabrice Emieux[a,b], E. de Vito[a,b], Frédéric Roux[a,b], Henri Mariette[a,c]

[a] Univ. Grenoble Alpes, F-38000 Grenoble, France

[b] CEA, LITEN, 17, rue des Martyrs, F-38054, Cédex 09 Grenoble, France

[c] CNRS, Institut Néel, 25, rue des Martyrs, F-38042, Grenoble, France

[*] Corresponding author: louis.grenet@cea.fr

***This is the peer reviewed version of the following article: "***Suzon, M. A. A., Grenet, L., Emieux, F., De Vito, E., Roux, F., & Mariette, H. (2019). Effect of Sb and Na Incorporation in Cu2ZnSnS4 Solar Cells. *physica status solidi (a)*, *216*(11), 1900070."***, which has been published in final form at* https://doi.org/10.1002/pssa.201900070 ***This article may be used for non-commercial purposes in accordance with Wiley Terms and Conditions for Use of Self-Archived Versions***

## Abstract

$Cu_2ZnSnS_4$-based solar cells suffer from limited power conversion efficiency and relative small grain size compared to selenium containing absorbers. Introduction of Na in $Cu_2ZnSnS_4$ absorbers either during the synthesis or after this step has been used to improve device performances and to determine whether its effect is based on structural properties improvement (grain size enhancement, better crystallization) or on opto-electronic properties improvement (defect passivation). In both cases, presence of Na in the absorber notably improves current and voltage of the solar cells, but the effect is more pronounced when Na is present during synthesis. Quantum efficiency analysis shows that these improvements can be related to longer minority carrier diffusion length and reduced absorber/buffer interface recombination. Introducing Na in the process mostly leads to preferential (112) orientation of the crystal which is clearly correlated with better device performances. Otherwise, the performance limitation due to small grain size has been discarded by the joint use of Sb and Na, which has a significant impact on grain size but does not affect solar cells efficiency.

## Introduction

Thin film photovoltaics based on kesterite absorber $Cu_2ZnSn(S,Se)_4$ (CZTSSe) have attracted a lot of attention in the last decade due to its potentiality of replacing $Cu(In,Ga)Se_2$ (CIGS) absorbers in the high efficiency thin film technology without using critical raw materials [1]. If first working kesterite devices were based on pure sulfur CZTS absorbers [2-3], most of the research effort with high performance devices have been dedicated in the past few years to CZTSe or Se-rich CZTSSe absorbers synthesized in presence of Se [4-7]. However, a recent renewed interest in pure sulfur CZTS based solar cells can be witnessed [8-9], and can be explained as follow: (i) CZTS exhibit a wider bandgap than CZTSe which will be translated into a lower cell to module efficiency loss [10], (ii) S is more abundant and less toxic than Se, particularly if $H_2S$ and $H_2Se$ are used to synthesize the absorbers [11] and (iii) sulfur based materials are generally better candidates in the current search for wide bandgap thin film materials usable in tandem solar cells applications [12].

However, to date the highest power conversion efficiency of devices made with CZTS absorbers (11.0% [8]) is still lower than the one with CZTSSe absorbers (12.6% [4]) or even with pure CZTSe absorbers (11.6% [5]) although they have a less favorable bandgap. One of the reason that can explain lower performances of sulfur devices lies in the smaller grains observed in these absorbers [13] which induces a higher concentration of detrimental grain boundaries [14]. Addition of Na in CZTS absorber has already shown beneficial effects in term of reduction of non-radiative recombination [15], enhancing the photovoltaic properties [16] and as well as in term of increasing the grain size [15]. However, in almost all the studies dealing with Na-doping in kesterite devices, Na is already present during the absorber synthesis [16], namely either introduced from the substrate [17] or in the precursor stack [15]. Thus it has an impact both on the material structural properties and on defect passivation. On the contrary, the introduction of Na after synthesis in CIGS technology has improved device performances but without modifying the crystallization of the layers [18]. In kesterite solar cells, it is thus not possible to determine whether Na improves device performances because of better structural (grain size, crystal quality) or opto-electronic (defect passivation) properties. On another hand, antimony (Sb) has already been used as surfactant to significantly increase the grain size in Cu(In,Ga)$Se_2$ technology in presence of Na [19] and may have the same role in CZTS absorbers.

In this study, we aim at improving performances of CZTS devices with the help of Na and Sb. Particularly, the effects of these elements on the absorber structural properties and the correlation with device properties are carefully discussed. In order to decouple the device improvement due to structural effects from the one due to opto-electronic properties, two routes have been in parallel conducted for Na incorporation: first Na has been added before the CZTS synthesis while in the second case, Na has been added after CZTS synthesis.

## 1 Experimental section

### *1.1 $Cu_2ZnSnS_4$ synthesis and solar cells fabrication*

CZTS based solar cells are fabricated from metallic stacks of precursors identical to those used for the CZTSe technology [20]. A Soda Lime Glass (SLG) substrate is first automatically cleaned and dried in a Pluritank USC120 MK4 from Novatec with successive ultrasonic and soap baths. A 500 nm Mo back electrode is then deposited by Direct Current (DC)-sputtering in an Alliance Concept Cluster Line equipment at 0.4 Pa and 2.1 W.cm$^{-2}$. Cu, Zn, Sn precursors are then DC-sputtered in a Perkin Elmer deposition chamber at 0.13 Pa and 1.3 W.cm$^{-2}$ without intentionally heating the substrate. Typical precursor stacks of Cu (5 nm ± 2 nm)/Sn (245 nm ± 20 nm)/Cu (190 nm ± 10 nm)/Zn (160 nm ± 10 nm) are used to synthesize Cu-poor Zn-rich CZTS absorber layers. The exact cationic composition of all the samples fabricated in this study is given in Supplementary Information Table S1.

2.5 x 2.5 cm$^2$ samples are then placed in a two zones resistive furnace. In the first zone, a sulfur source is heated at 200°C during the whole process while in the second zone, the sample is annealed at 550°C for 30 min (50 min is required to heat up the sample while natural cooling takes approximately 120 min). Sulfur vapors are transported in an Ar flow from the sulfur zone to the sample zone at a pressure of about 100 kPa. About 500 mg of sulfur is evaporated from the source during a single process.

Solar cells are completed with a 70 nm CdS buffer layer deposited by chemical bath. Cadmium acetate (1 mM), thiourea (5.1 mM), ammonium acetate (20 mM) and ammonia (0.3 mM) are stirred at 600 rpm and samples are immersed in the solution at 80°C for 15 minutes. A 50 nm/250 nm i-ZnO/ZnO:Al ($Al_2O_3$ 2 at%) window layer is RF-sputtered in a MRC2 chamber without intentional sample heating. Ni (50 nm) /Al (500

nm) grids are thermally evaporated on top of the solar cell. 0.5 x 0.5 $cm^2$ solar cells are manually scribed and no anti-reflecting coating is used on these samples.

With this process and by optimizing the sulfur source temperature (230°C), a maximum power conversion efficiency (PCE) of 5.9% has been obtained with a high $V_{OC}$ of 776 mV. Current-voltage (J-V) characteristics and External Quantum Efficiency (EQE) of this device are depicted in the supplementary Information (Fig. S1). In the following study, the sulfur source has been kept to 200°C in order to improve the reproducibility of the process, but limiting the efficiency in the 4% range.

### *1.2 Doping strategies*

In order to precisely control the amount of Na or Sb introduced in the absorber, diffusion of impurities from the SLG substrate have to be avoided. Thus, in the following experiments, a 300 nm $SiN_x$ diffusion barrier is systematically deposited by plasma assisted chemical vapor deposition in a STS 310PC reactor prior to Mo deposition.

Two strategies can be considered to improve a material with an extrinsic dopant. It can be either present during the material synthesis or it can be diffused inside the material once it is synthesized. These strategies are called Pre Absorber Synthesis (PAS) and Post Deposition Treatment (PDT) thereafter. In the case of Na addition in CZTS, both methods have been tested and compared in order to uncouple the structural effects from the opto-electronic effects of this element on the kesterite absorber. On the contrary, as Sb is only expected to enhance the grain size during the synthesis process, only PAS experiment have been carried out. Additionally, the joint effect of Sb and Na during the synthesis process has been studied.

In the case of PAS treatment (Fig. 1 (a)-(b)), NaF and Sb have been thermally evaporated in a homemade evaporation chamber equipped with Riber sources (ultimate vacuum $6.7x10^{-5}$ Pa) below (NaF) and above (Sb) the Cu/Sn/Cu/Zn precursor stack. Other configurations (NaF below precursor stack, Sb above precursor stack) are less successful in term of morphology (delamination, macroscopic inhomogeneities) or device performances. Different NaF and Sb thicknesses have been tested but with a maximum value of 40 nm and 20 nm respectively since CZTS starts to delaminate at higher NaF or Sb content. These samples are called PAS(NaXX) and PAS(SbYY) thereafter with an optional XX indicating the NaF thickness (in nm) and an optional YY the Sb thickness (in nm). To assess the joint effect of Na and Sb, a sample with 10 nm NaF (below the precursor stack) and 10 nm Sb (above the precursor stack) has been synthesized as well and is called PAS(Na+Sb) (Fig. 1 (c)).

In the case of PDT treatment, CZTS is first fabricated with the aforementioned method including the use of a $SiN_x$ diffusion barrier before thermal evaporation of NaF on top of the absorber (Fig. 1 (d)). A second annealing step at 350°C for 15 min under sulfur partial pressure (sulfur source at 200°C) is then performed to make Na diffuse into the absorber. NaF thicknesses up to 60 nm have been tested. These samples are called PDT(NaZZ) with an optional ZZ indicating the NaF thickness (in nm).

Finally, a sample with a $SiN_x$ barrier but without NaF nor Sb has been fabricated for reference and is later called Undoped (Fig. 1 (e)).

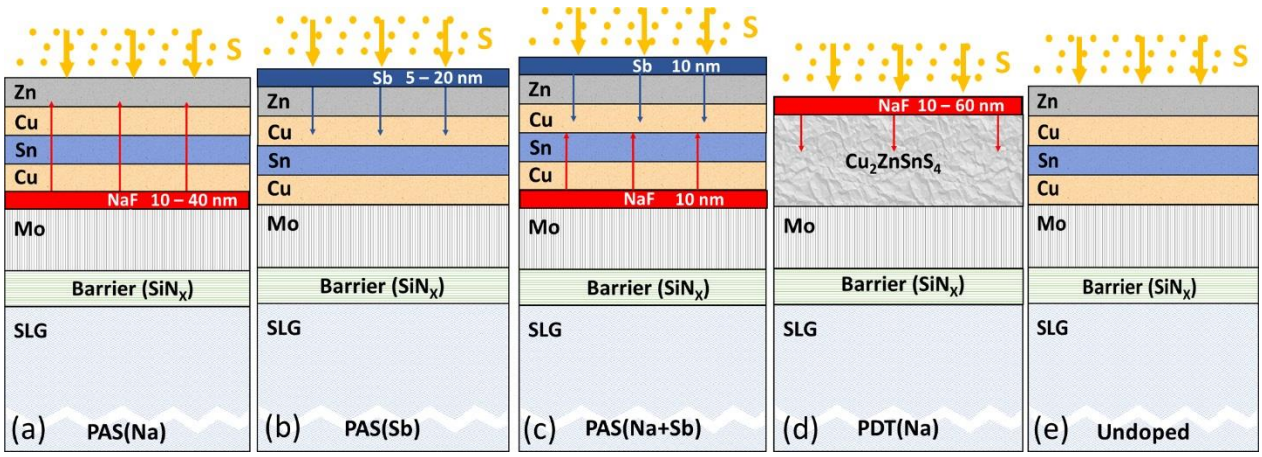


*Figure 1: Schematics of different configuration for Na and Sb incorporation. (a) PAS(Na) : NaF is deposited below the precursor stack, (b) PAS(Sb) : Sb is deposited on top of the precursor stack, (c) PAS(Na+Sb) : NaF is deposited below and Sb above the precusor stack, (d) PDT(Na) : NaF is deposited after NaF synthesis, (e) Undoped sample. For (a), (b) and (c) cases, Na or Sb diffuses during the 550°C annealing under S atmosphere. For (d), an additionnal annealing step at 350°C under S atmosphere is required.*

### *1.3 Characterization*

Scanning Electron Microscopy (SEM) images and Energy Dispersive Spectroscopy (EDS) measurements are made in a Zeiss LEO 1530 equipment. Preferential orientation of the crystal is measured by X-Ray Diffraction (XRD) in a D8 Advance Bruker AXS equipment and distribution of the elements throughout the depth of the absorber is determined by Time of Flight Secondary Ion Mass spectrometry (ToF-SIMS) in a IONTOF equipment. A Spectra-Nova's CT Series Solar Cell Tester is used to perform current-voltage (J-V) measurements under simulated AM1.5G spectrum (100 $mW.cm^{-2}$). All J-V measurements (light and dark) are performed at 25°C in a four-point probe configuration. External quantum efficiency (EQE) measurements are carried out in a ReRa Spequest equipment. Capacitance-Voltage (C-V) measurements are performed at 110 kHz and at room temperature with a 50 mV oscillating voltage in an Agilent HP E4980A Precision LCR meter.

## 2 Results and discussion

### *2.1 Incorporation of Na and Sb*

ToF-SIMS has been used on selected samples (PAS(Na10), PDT(Na40), PAS(Sb10) chosen for their optimized photovoltaic properties shown later) to determine whether and where Na and Sb are incorporated in CZTS absorbers. These profiles are shown in Fig. 2(a) for Na and (b) for Sb. First it is remarkable that both Na incorporation strategies (PAS and PDT) increase significantly (more than one order of magnitude of counts raise) the Na amount in the absorber compared to the undoped sample. The migration of a small amount of Na (with similar significant variation of SIMS counts with and without barrier) from the substrate through a diffusion barrier has already been observed using a $SiO_X$ barrier [21], but it has been demonstrated that this low amount of Na does not play a significant role on PV properties [21].

In more details, PDT sample shows a relatively flat Na profile with almost no Na in the Mo back contact (comparable to the undoped sample) and only limited signal increases at the front surface, while PAS sample exhibits a more U-shape profile, with higher Na amount at the front and back interfaces (as well

as in the Mo back electrode). This Na distribution is consistent with other works [15] showing that Na mostly accumulates at the absorber surfaces and grain boundaries. A clearer picture of the Na content in the 3 samples can be found in Fig. S2(a) where the Na signal has been integrated in 3 domains: the front surface, the bulk CZTS and the Mo back electrode. It shows that both doped samples (PAS and PDT) have a large and similar amount of Na in the bulk absorber but only PAS sample has a significant increase in Na content at the front surface and in the Mo electrode. This latter result is in agreement with the presence of Na during the synthesis step.

In Fig. S2(b), the F profile is also drawn and clearly reveal that F is present as well in the absorber after both PAS and PDT treatments and its impact on material properties could be discussed as well. It is however out of the scope of this study.

As far as Sb is concerned, the picture (Fig. 2 (b)) is quite different: first, Sb detection is at the detection limit for on the undoped sample. In the sample synthesized with Sb, only a minor increase in the Sb signal can be found close to the back interface but with an order of magnitude similar to the noise measured in ToF-SIMS. It can thus be concluded that in the case of Sb assisted synthesis, no Sb remains in the absorber after the process.

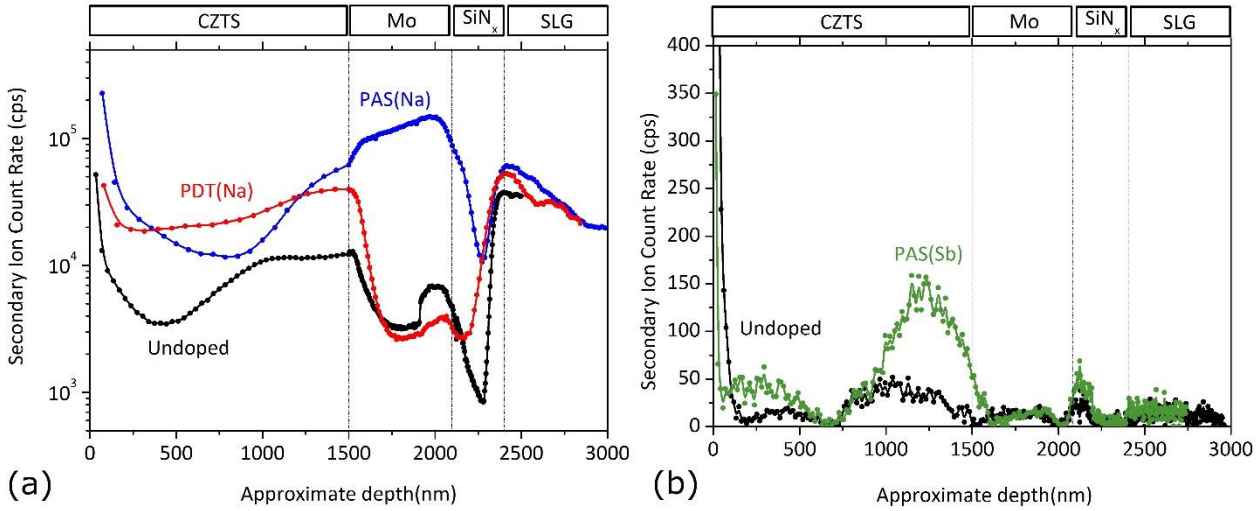


*Figure 2: (a) Na ToF-SIMS profiles in CZTS/Mo/$SiN_x$/SLG structures and (b) Sb ToF-SIMS profiles in CZTS/Mo/$SiN_x$/SLG structures. The position of the different layers (CZTS, Mo, $SiN_x$, SLG) is estimated from the Cu, Zn, Sn, S, Mo, Si N and O profiles not shown.*

### *2.2 Effect on the absorber structural properties*

SEM top view images of the samples are shown in Fig. 3 (a)-(e). Undoped sample (Fig. 3 (a)) exhibits relatively small grains (few hundreds of nanometers) with various shapes (from circular to more faceted grains). The addition of Na during the synthesis (PAS(Na), Fig. 3 (b)) slightly increases the grain size but more remarkably changes the morphology of the grains, which become more angular. On the PDT(Na) sample (Fig. 3 (c)), an additional layer with very small grains can be found at the absorber surface. It is attributed to remaining NaF after the process but underneath, one can distinguish CZTS grains which are not affected by the additional treatment. Addition of Sb alone during the synthesis step (PAS(Sb), Fig. 3 (d)) does not affect the grain size and leads to slightly more circular grains whereas the joint addition of Na and Sb during the synthesis (PAS(Na+Sb) Fig. 3 (e)) drastically enhances the grain size (grain sizes of few

micrometers can be observed). This latter result is further confirmed by the comparison of the cross-section images of the undoped sample (Fig. 3 (f)) and the PAS(Na+Sb) sample (Fig. 3 (g)).

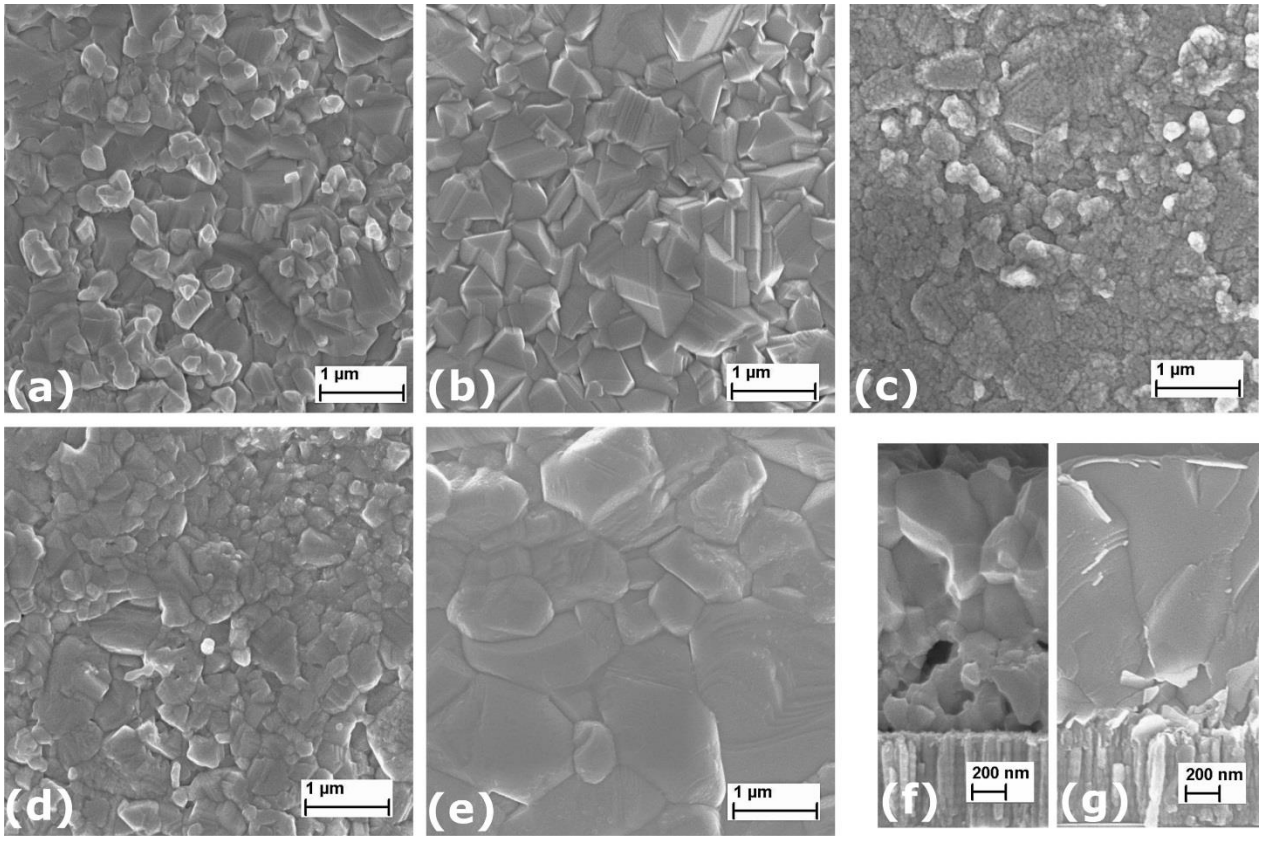


*Figure 3: SEM top view of (a) undoped sample, (b) PAS(Na), (c) PDT(Na), (d) PAS(Sb), (e) PAS(Na+Sb) and SEM cross section of (f) undoped sample, (g) PAS(Na+Sb).*

The modification of the grain morphology with extrinsic dopants (Na and Sb) can be driven by preferential orientation of the films [22]. Thus, XRD scans have been performed on all samples focusing on the (112) and (220,204) peaks located at about 28° and 47° respectively. These scans are shown in Fig. S3. Preferential (112) orientation of the thin films can be estimated by calculating the ratio of the area located beneath the (112) and (220,204) peaks respectively. The intensity ratio of both peaks ($I_{112}/I_{220,204}$) is depicted in Fig. 4. Undoped sample as well as PAS(Sb) and PDT(Na) samples exhibit a ($I_{112}/I_{220,204}$) ratio very close to a film with randomly distributed grains [22]. On the contrary, the presence of Na during synthesis (PAS(Na) samples) notably increases the (112) orientation of the films up to 15 nm of NaF. Above this value, texturization of the films decreases again to randomly oriented grains. In the case of PAS(Na+Sb) sample, the ($I_{112}/I_{220,204}$) ratio is almost equal to the ratio from sample PAS(Na10). In the case of selenization process, (112) crystal orientation in the presence of Na during synthesis process has been pointed out [22] and is correlated to the formation of a liquid $Na_2Se_x$ phase during the growth. However, the decrease in (112) preferred orientation at high NaF thicknesses for PAS(Na) samples is not elucidated.

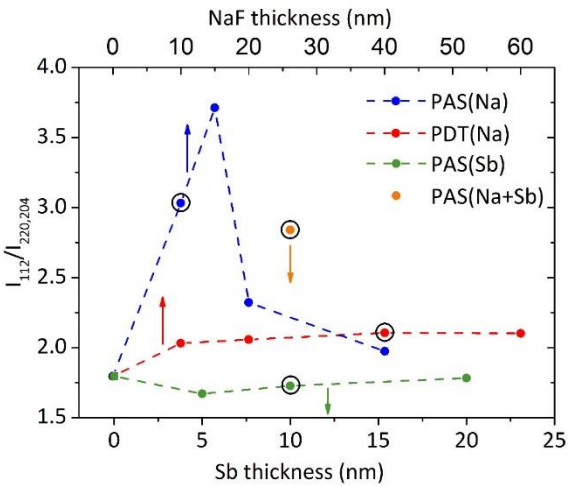


*Figure 4: Ratio of the (112) on (220.204) XRD peak intensities as function of the amount of material (Sb or NaF) used during (PAS) or after (PDT) synthesis. Dotted line are guide for the eyes. The PAS(Na+Sb) is synthesized with 10 nm NaF and 10 nm Sb. Surrounded data points corresponds to SEM pictures of Fig. 2.*

### *2.3 Impact on devices properties*

9 solar cells have been fabricated on each sample and measured under AM1.5 simulated spectrum. Photovoltaic properties (Power Conversion Efficiency PCE, Fill Factor FF, Open-circuit Voltage $V_{OC}$ and Short Circuit Current $J_{SC}$) of the solar cells are presented in boxplot in Fig. 5.

With the addition of Na (either by PAS or PDT) in CZTS absorbers, PCE of the solar cells are significantly improved with a roughly equal share coming from a higher $V_{OC}$ and a higher $J_{SC}$; the positive impact on FF being less substantial. This behavior is more pronounced for PAS samples where an optimum NaF thickness of 15 nm is found, leading to PCE improvement higher than 2% absolute. PCE decreases again at higher Na content and the notable FF drop with 40 nm NaF is due to the fact that CZTS layer starts to peel off. The picture for PDT samples is quite different: PCE (and all photovoltaic properties) increases with NaF thickness but to a lower extent than in the case of PAS and with a saturation of the effect at about 20 nm of NaF.

On the contrary, the use of Sb alone in the process does not affect any photovoltaic properties. Although the joint use of Na and Sb leads to an impressive increase in the absorber grain size, it is not translated into a significant increase of the photovoltaic properties of the device. Indeed, they are very similar to the properties of the PAS(Na10) sample and the gain in PCE can thus be attributed solely to the presence of Na. From this part, it can be concluded that the grain size is currently not a key parameter for the limitation of the CZTS-based devices performances.

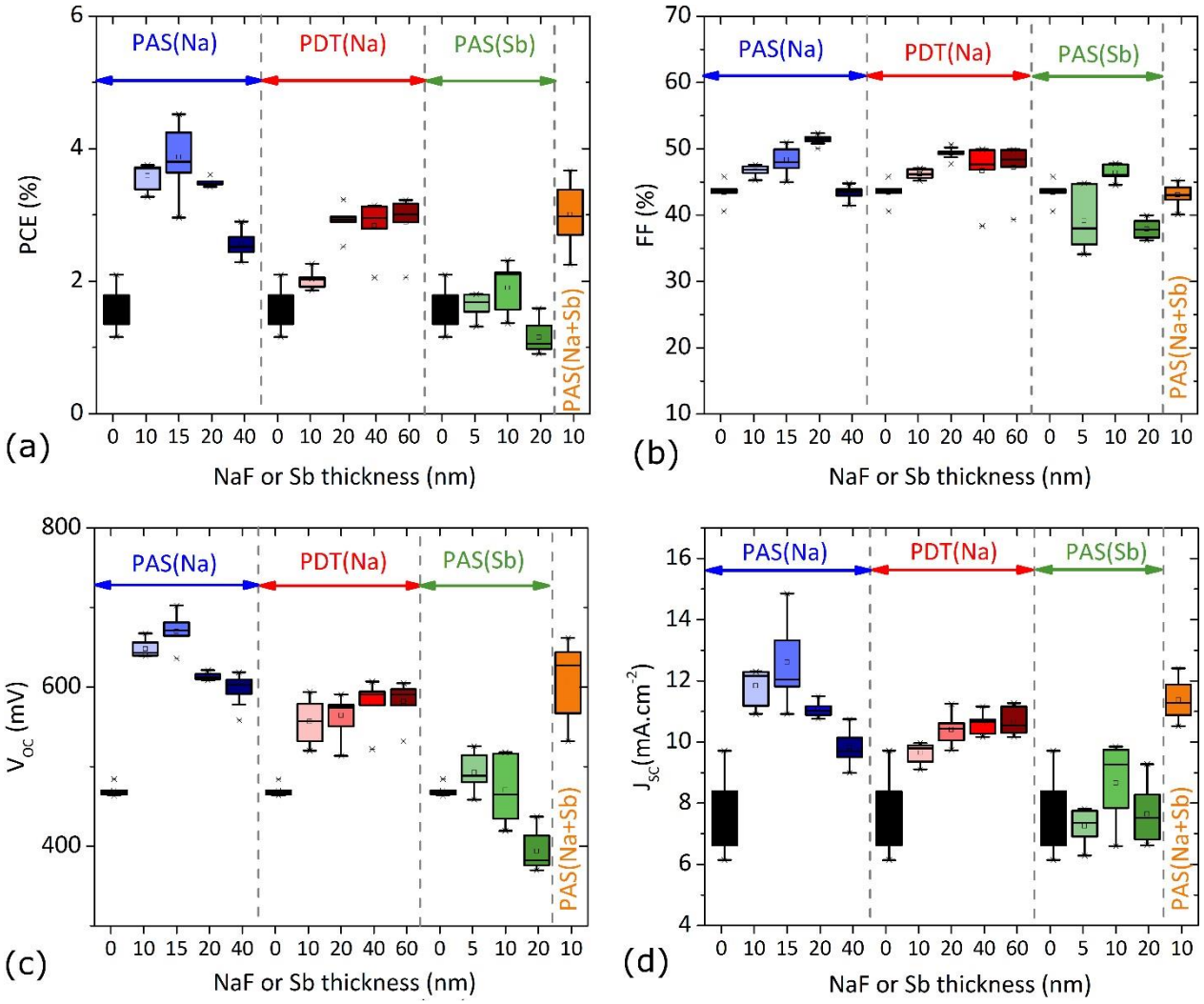


*Figure 5: Photovoltaic properties ((a) PCE, (b) FF, (c) $V_{OC}$, (d) $J_{SC}$) of samples with PAS(Na), PDT(Na), PAS(Sb) and PAS(Na+Sb) treatments as function of the material (NaF or Sb) thickness.*

### *3.4 Role of Na on photovoltaic properties*

To further understand the origin of the photovoltaic properties ($J_{SC}$ and $V_{OC}$) improvement with Na addition in the absorber layer, EQE and C-V measurements have been carried out and are depicted in Fig. S4.

EQE spectra have been fitted with the simulation software e-ARC [23] developed at Gifu University (Japan) in order to extract current losses in the back electrode (Mo+$MoS_2$), in the front electrode (ZnO/ZnO:Al), in the buffer layer (CdS) and by reflection. e-ARC software allows as well to estimate the current loss due to the recombination either at the absorber/buffer interface (which is translated in the EQE spectrum in a low quantum efficiency at short (< 600 nm) wavelengths [24]), or in the absorber bulk due to insufficient minority carrier collection length (which is translated in the EQE spectrum in a low quantum efficiency at long (> 600 nm) wavelengths [24]). Results of the simulations are depicted in Fig. 6 (a) along with the evolution of the $J_{SC}$ for the same solar cells (top). Losses in the back electrode (Mo + $MoS_2$) as well as front optical losses (reflection + absorption in the CdS/ZnO/ZnO:Al layers) are significant but roughly constant and cannot explain the improvement of the devices with Na. In the case of PAS process, a large decrease

in the current loss at the interface (IF) due to reduced recombination is witnessed and can explain a 4 $mA.cm^{-2}$ current gain in the PAS(Na15) sample, while the $J_{SC}$ gain due to better collection is limited to less than 2 $mA.cm^{-2}$ (PAS(Na15)) and is null for PAS(Na40). On the contrary, in the case of PDT process, most of the improvement comes from the bulk losses reduction (up to 3.25 $mA.cm^{-2}$) while the IF losses reduction is roughly constant (~ 1.7 $mA.cm^{-2}$ current gain). The larger surface improvement for PAS(Na) samples can be related to the more important amount of Na found close to the CZTS/CdS interface in this latter case (Fig. S2 (a)).

By analyzing the C-V data, it is possible to determine an apparent carrier concentration ($N_{CV}$) and the depletion width (W) in the absorber [25]. Fig. 5(b) top shows $N_{CV}$ extracted at 0 V as function of the NaF thickness. The increase in carrier concentration of almost one order of magnitude with addition of Na in the process has already been observed in literature [26]. However, this higher carrier concentration can only account for about 10 mV of $V_{OC}$ improvement [27] and cannot explain alone the 200 mV voltage gain in the devices.

Assuming that the carrier collection length is equal to the sum of the minority carrier diffusion length ($L_D$) and W [28], the combination of these experiments allow to estimate $L_D$ as shown in Fig. 6(b) (bottom). In the undoped sample, $L_D$ ~ 0 nm has been found which means that the collection length extracted from EQE is equal to W extracted from C-V. In the case of PDT(Na), $L_D$ increases with NaF thickness up to 100 nm while in the case of PAS(Na), a maximum value of almost 300 nm is found for 15 nm of NaF. These values are consistent with other publications [29,30].

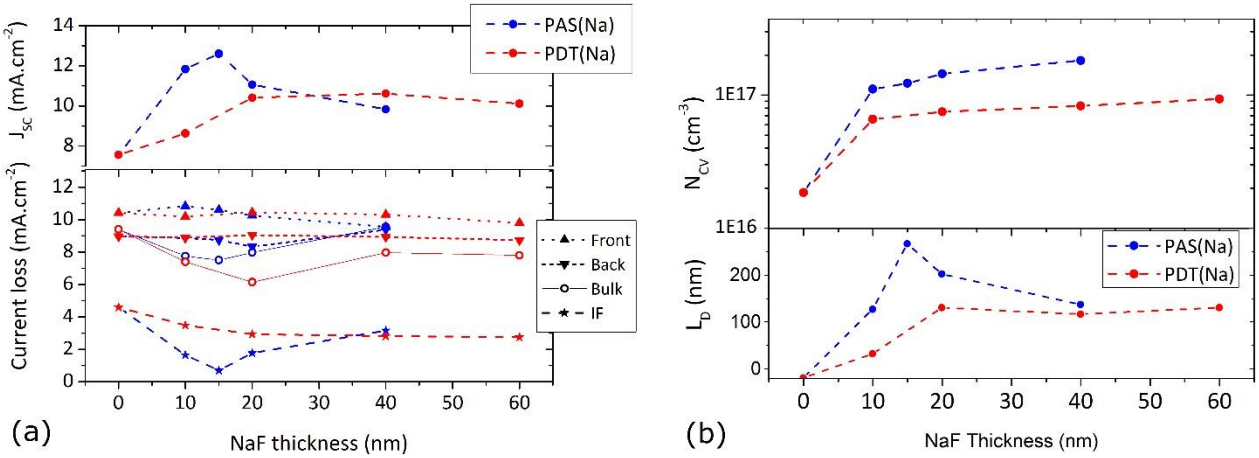


*Figure 6: (a) Top: evolution of the $J_{SC}$ of the best solar cells as function of the NaF thickness used in the PAS (blue) and PDT (red) processes. Bottom: evolution for the same solar cells of the current loss in the front electrode (reflection + absorption in ZnO:Al/ZnO/CdS), the back electrode (absorption in $MoS_2$/Mo), in the bulk of the absorber due to insufficient collection length and at the CZTS/CdS interface due to recombination. (b) Top: Evolution of the apparent carrier density measured by C-V as function of the NaF thickness used in the PAS (blue) and PDT (red) processes. Bottom: Evaluation of the carrier diffusion length in the CZTS as function of the NaF thickness used in the PAS (blue) and PDT (red) processes.*

The contribution of the bulk and IF recombination reduction to the $V_{OC}$ gain is not straightforward and cannot be directly estimated from the ratio of the bulk and IF current losses estimated from EQE analysis. Indeed, due to a small type inversion in the CZTS surface at $J_{SC}$ (our sample preparation is similar to the "75°C as deposited" condition of Ref. [31]) leading to a large photo-injection of minority carrier (holes), the position of maximum recombination is close to the surface [25]. At higher forward voltage ($V_{OC}$), the band alignment is changed (depending on whether the quasi-Fermi level is pinned or not) and the position

of maximum recombination can be different [25]. Thus IF and bulk recombination contribution to the diode current (and thus to the $V_{OC}$) cannot be directly extracted from measurements at $J_{SC}$.

The bulk contribution to the $V_{OC}$ gain can however been tentatively estimated with a simple model. In the supplementary information of Ref. [32], Hages & al. have simulated the dependence of $V_{OC}$ on minority carrier lifetime in kesterite solar cells for different back and front surface recombination velocities ($S_B$ and $S_F$ respectively). By assuming a constant electron mobility $\mu$ = 100 $cm^2/V.s$ [33] and using the Einstein relation, it is possible to re-plot these simulated results as function of $L_D$ and the superimposition with our experimental data is reasonable (Fig. 7 (a)). According to these simulations, it is clear that with such $L_D$ values, most of the $V_{OC}$ deficit (expressed as the difference with the maximum open-circuit voltage achievable in the Schockley Queisser limit: $V_{OC\text{-}SQ}$ = 1168 mV for the 1.45 eV bandgap CZTS absorber) arises from bulk recombination. For $L_D$ = 100 nm, $V_{OC}$ deficit > 500 mV while decreasing $S_{IF}$ from $10^6$ $cm^{-1}$ to $10^2$ $cm^{-1}$ is only translated to a 40 mV increase in $V_{OC}$. Thus, the $V_{OC}$ gain due to the addition of Na in the absorber comes mainly from improved bulk properties. One can notice that experimental data points better fit with devices with large interface recombination (this trend is even more obvious if smaller mobility is considered), but this large interface recombination is not limiting the $V_{OC}$ of the devices at this point.

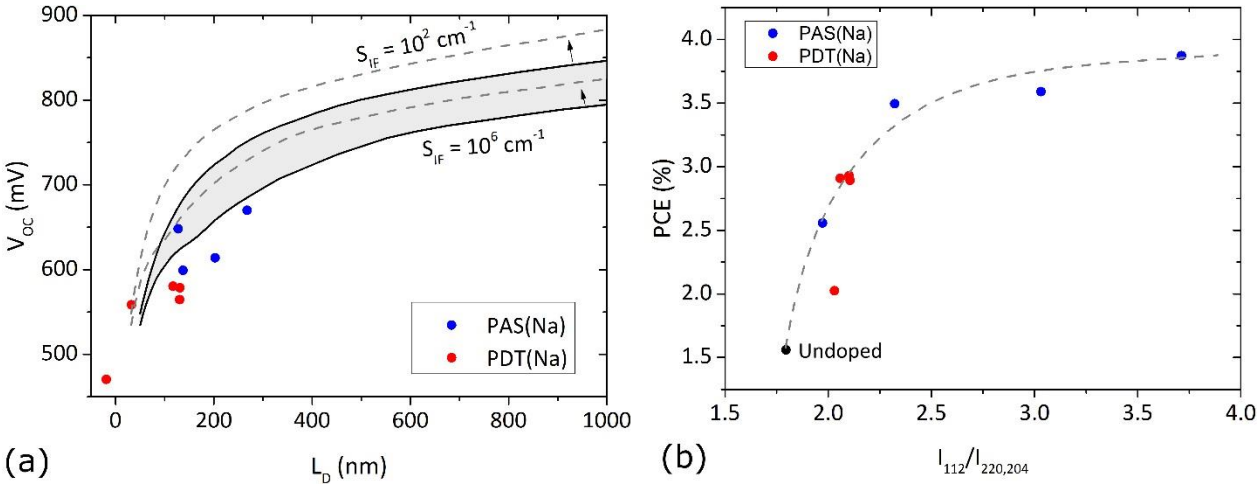


*Figure 7: (a) $V_{OC}$ of the CZTS-based solar cells for both PAS(Na) and PDT(Na) processes as function of $L_D$ estimated from EQE simulations. The solid lines represents device simulation (extracted from Ref. [32] for a 1.45 eV bandgap and assuming $\mu$=100 $cm^2/V.s$) with different CZTS/CdS ($S_{IF}$) and Mo/CZTS ($S_B$) interface recombination velocities: for the top curve, $S_{IF} = 10^2$ $cm^{-1}$ and $S_B = 10^2$ $cm^{-1}$ and for the bottom curve, $S_{IF} = 10^6$ $cm^{-1}$ and $S_B = 10^7$ $cm^{-1}$. Recombination at the Mo/CZTS interface has a minor impact since the carrier collection length is smaller than the absorber thickness. Dashed lines represents same simulations assuming $\mu$=40 $cm^2/V.s$.(b) PCE of the CZTS-based solar cells for both PAS(Na) and PDT(Na) processes as function of the preferential orientation of the absorber. The dashed line is a guide for the eyes.*

Interestingly, Fig. 7 (b) shows a clear increase in the PCE of the devices with the preferential (112) orientation of the absorber layer. An exactly similar trend is noticed for $V_{OC}$. The impact of the crystalline orientation on kesterite device performances is very rarely discussed. In Ref. [22] an opposite behavior is obtained for selenium based-devices and similarly, in CIGS technology, absorbers with preferred (220/204) orientation give better performances [34,35]. This latter effect is attributed to the reduction of non-radiative recombination center close to the absorber surface.

As far as CZTS-based devices are concerned, the picture is quite different since the presence of Na during absorber synthesis favors the (112) orientation which is then translated into better device performances.

Here can lie one of the reason explaining the better performances of PAS(Na) samples compared to PDT(Na) samples as already observed in literature [21]. Effect of preferred orientation can change both the presence of recombination center close to the interface but as well the nature of the grain boundaries within the absorber. A reduced recombination on the grain boundaries in the absorber should be as well translated in longer $L_D$ as observed in PAS(Na) samples.

## 3 Conclusion

In this study, the impact of Na and Sb on the structural an opto-electronic properties of CZTS-based solar cells has been studied starting from a process of sulfurization of metallic precursors leading to maximum device efficiencies of 5.9%.

It has first been shown that the separate use of Na or Sb during the synthesis process has no relevant effect on the CZTS grain size while their joint use drastically improve the crystallization. Additionally, the presence of limited amount of Na during synthesis favors the (112) preferential orientation of the films contrary to Sb which does not affect this property.

Devices made with these absorbers reveal that Na is very beneficial for photovoltaic performances contrary to Sb which has no impact. Particularly, the large grain size enhancement with Sb + Na is not translated into performances increase and thus small grain size is not seen as a limitation for solar cell performances. It has been demonstrated as well that larger performance enhancement is obtained when Na is present during the CZTS synthesis and thus, both structural and opto-electronic improvements of the absorber are responsible for higher efficiency.

Further analysis of the effect of Na in the photovoltaic properties shows that it is beneficial both in term of $J_{SC}$ and $V_{OC}$. In the first case, the improvement arises almost to an equal share for reduction in surface and bulk recombination, with a more pronounced interface effect when Na is present during synthesis, which has been attributed to a more important amount of Na close to the CZTS/CdS interface. As far as $V_{OC}$ is concerned, its deficit is mostly reduced due to increased minority carrier diffusion length. The required presence of Na during synthesis to achieve the best performances can be partly explained by the preferred induced (112) orientation of the absorber which leads to better PV properties.

## Supporting Information

Supporting Information is available on XXX or from the authors.


## Acknowledgements

This research was supported by the Laboratoire d'excellence LANEF in Grenoble (ANR-10-LABX-51-01) and the H2020 Programme under the project STARCELL (H2020-NMBP-03-2016-720907)


## References


[1] I. Repins, N. Vora, C. Beall, S.-H. Wei, Y. Yan, M. Romero, G. Teeter, H. Du, B. To, M. Young, R. Noufi, , *MRS Online Proc.* **2011,** *1324*.
[2] H. Katagiri, M. Nishimura, T. Onozawa, S. Maruyama, M. Fujita, T. Sega, T. Watanabe, *Proc. Power Conversion Conf.*, **1997**, *2*, 1003-1006.
[3] H. Katagiri, *Thin Solid Films*, **2005**, *480*, 426-432.
[4] W. Wang, M.T. Winkler, O. Gunawan, T. Gokmen, T.K. Todorov, Y. Zhu, D.B. Mitzi, *Adv. Energy Mater.*, **2014**, *4(7)*, 1301465.

[5] Y.S. Lee, T. Gershon, O. Gunawan, T.K. Todorov, T. Gokmen, Y. Virgus, S. Guha, *Adv. Energy Mater.*, **2015**, *5(7)*, 1401372.
[6] S. Giraldo, E. Saucedo, M. Neuschitzer, F. Oliva, M. Placidi, X. Alcobé, V. Izquierdo-Roca, S.Kim, H.Tampo, H. Shibata, A. Perez-Rodriguez, P. Pistor, *Energy Environ. Sci.*, **2018**, *11(3)*, 582-593.
[7] S.G. Haass, C. Andres, R. Figi, C. Schreiner, M. Bürki, Y.E. Romanyuk, A.N. Tiwari, *Adv. Energy Mater.*, **2018**, *8(4)*, 1701760.
[8] C. Yan, J. Huang, K. Sun, S. Johnston, Y. Zhang, H. Sun, A. Pu, M. He, F. Liu, K. Eder, L. Yang, J.M. Cairney, N. J. Ekins-Daukes, Z. Hameiri, J.A. Stride, S. Chen, M.A. Green, X. Hao, *Nat. Energy*, **2018**, *3(9)*, 764.
[9] T. Ericson, F. Larsson, T. Törndahl, C. Frisk, J. Larsen, V. Kosyak, C. Hägglund, S. Li, C. Platzer-Björkman, *Solar RRL*, **2017**, *1(5)*, 1700001.
[10] V. Bermudez, A. Perez-Rodriguez, *Nat. Energy*, **2018**, *3(6)*, 466.
[11] V.M. Fthenakis, P.D. Moskowitz, *Prog. Photov. Res. Appl.*, **2000**, *8(1)*, 27-38.
[12] M.A. Green, *Nat. Energy*, **2018**, *1(1)*, 15015.
[13] H.R. Jung, S.W. Shin, M.P. Suryawanshi, S.J. Yeo, J.H. Yun, J.H. Moon, J.H. Kim, *Sol. Energy*, **2017**, *145*, 2-12.
[14] L. Grenet, M.A.A. Suzon, F. Emieux, F. Roux, *ACS Appl. Energy Mater.*, **2018**, *1(5)*, 2103-2113.
[15] T. Gershon, B. Shin, N. Bojarczuk, M. Hopstaken, D.B. Mitzi, S. Guha, *Adv. Energy Mater.*, **2015**, *5(2)*, 1400849.
[16] T. Mise, S. Tajima, T. Fukano, K. Higuchi, T. Washio, K. Jimbo, H. Katagiri, *Prog. Photov. Res. Appl.*, **2016**, *24(7)*, 1009-1015.
[17] G. Altamura, C. Roger, L. Grenet, J. Bleuse, H. Fournier, S. Perraud, H. Mariette, *Mater. Res. Soc. Symp. Proc.*, **2013**, *1538*, 103-106.
[18] D. Rudmann, A.F. Da Cunha, M. Kaelin, F. Kurdesau, H. Zogg, A.N. Tiwari, G. Bilger, *Appl. Phys. Lett.*, **2004**, *84(7)*, 1129-1131.
[19] Y. Yatsushiro, H. Nakakoba, T. Mise, T. Kobayashi, T. Nakada, *Jpn. J. Appl. Phys.*, **2012**, *51*, 10NC25
[20] L. Grenet, M.A.A. Suzon, F. Emieux, F. Roux, *J. Ren. Sust. Energy*, **2018**, *10(4)*, 043503.
[21] C. Andres, T. Schwarz, S.G. Haass, T.P. Weiss, R. Carron, R. Caballero, R. Figi, C. Schreiner, M. Bürki, A.N. Tiwari, Y.E. Romanyuk, *Sol. Energy*, **2018**, *175*, 94-100.
[22] C.J. Hages, M.J. Koeper, C.K. Miskin, K.W. Brew, R. Agrawal, *Chem. Mater.*, **2016**, *28(21)*, 7703-7714.
[23] T. Hara, T. Maekawa, S. Minoura, Y. Sago, S. Niki, H. Fujiwara, *Phys. Rev. Applied*, **2014**, *2*, 034012. This free software can be downloaded freely at https://unit.aist.go.jp/rcpv/cie/service/index.html.
[24] C.J. Hages, N.J. Carter, R. Agrawal, *J. Appl. Phys.*, **2016**, *119*, 014505
[25] R. Scheer, H.W. Schock, Chalcogenide photovoltaics: physics, technologies, and thin film devices, *John Wiley & Sons*, **2011.**
[26] A. Nagaoka, H. Miyake, T. Taniyama, K. Kakimoto, Y. Nose, M.A. Scarpulla, K. Yoshino, *Appl. Phys. Lett.*, **2014**, *104(15)*, 152101.
[27] F. Pianezzi, P. Reinhard, A. Chirilă, B. Bissig, S. Nishiwaki, S. Buecheler, A.N. Tiwari, *Phys. Chem. Chem. Phys*., **2014**, *16(19)*, 8843-8851.
[28] A. Nakane, H. Tampo, M. Tamakoshi, S. Fujimoto, K. M. Kim, S. Kim, H. Shibata, S. Niki, H. Fujiwara, *J. Appl. Phys.*, **2016**, *120*, 064505.
[29] L. Grenet, R. Fillon, G. Altamura, H. Fournier, F. Emieux, P. Faucherand, S. Perraud, *Sol. Energy Mater. Sol. Cells*, **2014**, *126*, 135-142.
[30] C. Frisk, T. Ericson, S.Y. Li, P. Szaniawski, J. Olsson, C. Platzer-Björkman, *Sol. Energy Mater. Sol. Cells*, **2016**, *144*, 364-370.
[31] A. Crovetto, A. Cazzaniga, R.B. Ettlinger, J. Schou, O. Hansen, *Sol. Energy Mater. Sol. Cells*, **2018**, *187*, 233-240.
[32] C.J. Hages, A. Redinger, S. Levcenko, H. Hempel, M.J. Koeper, R. Agrawal, D. Greiner, C.A. Kaufmann, T. Unold, *Adv. Energy Mater.*, **2017**, *7(18)*, 1700167.

[33] H. Hempel, R. Eichberger, I. Repins, T. Unold, *Thin Solid Films*, **2018**, *666*, 40-43.
[34] M.A. Contreras, M.J. Romero, R. Noufi, *Thin Solid Films*, **2006**, *511*, 51-54.
[35] J.H. Yoon, W.M. Kim, J.K. Park, Y.J. Baik, T.Y. Seong, J.H. Jeong, *Prog. Photov. Res. Appl.*, **2014**, *22(1)*, 69-76.